

# Supplementary Information for:

## Anodic Molecular Hydrogen Formation on Cu and Ru Electrodes

Søren B. Scott, Albert K. Engstfeld, Zenonas Jusys, Degenhart Hochfilzer, Nikolaj Knøsgaard, Daniel B. Trimarco, Peter C.K. Vesborg, R. Jürgen Behm, Ib Chorkendorff

### Contents

- Experimental Details
  - Materials
  - Sample Preparation
  - Electrochemistry – Mass Spectrometry
  - Calibration
  - Electrochemical Procedures
- Supplementary Figures
  - Figure S1. Data from main-text Figure 1 vs time.
  - Figure S2 and Table S1. Quantification details for Ru(0001)
  - Figure S3. Tilt on Cu and Pt
  - Figure S4. Quantification on Cu
  - Figure S5. Hydrogen adsorption and desorption on Cu vs pH
  - Figure S6. Free energy sketches for H<sub>2</sub>
  - Figure S7. RE calibration (using Pt) in EC-MS
  - Figure S8 STM image of Ru(0001) of the as prepared surface and after EC.
  - Figure S9 First cycles recorded on Ru(0001) in 0.1 M HClO<sub>4</sub>

## Experimental Details

### Materials

The Ru(0001) single crystals were purchased from Mateck GmbH (Purity 99.9999 %, diameter 10 mm, thickness 2 mm, hat shaped). The Ru(0001) single crystal was prepared under UHV conditions (see below). The 0.1 M HClO<sub>4</sub> electrolyte used for the electrochemical characterization of the Ru(0001) electrodes was prepared from milliQ water (18.2 Ohm, Millipore A/S) and HClO<sub>4</sub> (Meck Suprapure 70%).

The polycrystalline copper stub was cut to 5 mm in diameter and 3 mm height from a 99.999% pure Cu rod from Merck A/S. The 0.1 M KOH electrolyte used for characterization the Cu(poly) was prepared from milliQ water and Suprapur (99.99%) potassium hydroxide monohydrate from Sigma Aldrich.

### Sample preparation

The Ru(0001) electrodes were prepared under UHV conditions in a setup described elsewhere<sup>1</sup>. The electrode preparation was adapted from a previous work, which provided high quality surfaces and well defined electrochemical features in 0.5 M H<sub>2</sub>SO<sub>4</sub> electrolyte<sup>2</sup> were treated with three cycles of Ar<sup>+</sup> sputtering (pAr = 3·10<sup>-5</sup> mbar, I = 4 μA/cm<sup>2</sup>, t = 30 min,) and flash annealing to 1600 K in less than 20 s. This allows for complete removal of electrolyte residues from the previous experiment. Subsequently the electrodes were exposed to seven cycles of flash annealing to 1600 K and dosing 10 L of O<sub>2</sub> (pO<sub>2</sub> = 1.33·10<sup>-6</sup> mbar, t = 10 s) at T < 600 K, to remove carbon impurities segregating to the electrode surface during the annealing steps and to form large atomically flat terraces as shown in an exemplary STM image in the supporting information (**Figure S8**). Note that Ru(0001) is usually prepared under UHV conditions. Another non UHV approach to prepare single crystals, requires annealing fo the electrodes by inductive heating under inert gas<sup>3</sup>.

The Cu(poly) disk was mechanically polished by hand for two minutes using a polishing cloth and 0.3 μm alumina paste. It was then sonicated at room temperature for 10 minutes in milliQ water, 10 minutes in ethanol, and another 10 minutes in milliQ water.

### Electrochemistry - mass spectrometry setups

The Ru(0001) electrodes were investigated in an electrochemical flow cell combined with a DEMS, described in detail in Reference <sup>4</sup>. The DEMS cell was slightly modified, such that the inlet hose was passed through liquid N<sub>2</sub>. This allowed for condensation of H<sub>2</sub>O diffusing through the DEMS membrane, which reduces the background pressure in the DEMS system from 3·10<sup>-5</sup> mbar to 1·10<sup>-6</sup> mbar and thus results in a better m/z = 2 signal to noise ratio. The potential was controlled with a Pine AFRDE5 Bi-potentiostat and the data was acquired with an in-house programmed software. The electrolyte was provided from an electrolyte supply bottle which is deaerated with N<sub>2</sub> (Westfalen 6.0).

The Cu(poly) electrodes were investigated in a stagnant thin-layer cell combined with a chip-based electrochemistry - mass spectrometry (chip EC-MS) setup as described in Reference <sup>5</sup>. Briefly, a silicon microchip (Spectro Inlets A/S) containing a perforated membrane and a 60 nl (3  $\mu\text{m}$  high) internal volume functions as a microscopic headspace to a 2  $\mu\text{l}$  (100  $\mu\text{m}$  high) working volume of electrolyte between the chip's membrane and the electrode surface. A capillary connecting the chip's internal volume to the vacuum system delivers gaseous products to the mass spectrometer (Quadrupole Mass Analyzer 420, Pfeiffer A/S) without differential pumping, enabling high sensitivity. The potential and current were controlled and measured using a BioLogic SP-150 potentiostat. The datasets were combined and analyzed using an in-house python package available at [http://github.com/ScottSoren/EC\\_MS](http://github.com/ScottSoren/EC_MS).

### Calibration

With the DEMS setup, a homemade RHE electrode was used as reference. The  $\text{H}_2$  signal at  $m/z=2$  was calibrated by determining the  $K^*$  factor, which relates the Faraday current to the mass spectrometry signal via  $K = n^*j_{\text{QMS}}/j_{\text{F}}$ , where  $n$  is the number of electrons,  $j_{\text{QMS}}$  the current from the  $m/z$  signal and  $j_{\text{F}}$  the Faraday current in the CV. The value is finally determined from the HER region of the negative going scan of the CV at high overpotentials.

For the chip EC-MS setup, a Hg/HgSO<sub>4</sub> reference electrode from SI Analytics was used and calibrated against the RHE in the same setup using a platinum electrode and saturating the 0.1 KOH electrolyte with  $\text{H}_2$  through the chip (**Figure S7**). The  $\text{H}_2$  signal at  $m/z=2$  was calibrated using a series of constant-current steps from -100  $\mu\text{A}$  to -1  $\mu\text{A}$  using the same Pt electrode. The sensitivity factor,  $F_{\text{M}2}^{\text{H}2}$  was determined to be 2.71 C mol<sup>-1</sup> by the line of best fit through the steady-state signal (in A) vs the electrochemical hydrogen production rate (in mol s<sup>-1</sup>) for these constant-current steps, assuming 100% faradaic efficiency for HER on Pt (**Figure S7**).

### Electrochemical procedures

The Ru(0001) electrode was first cycled in a potential range of 0.10 to 0.90 V and subsequently cycled between -0.20 to 0.90 V. In some cases the CV changes after the low potential excursion, but does not change in subsequent cycles, independent of the applied potential limits (**Figure S9**).

The Cu(poly) electrode was cycled at 50 mV/s for 100 cycles in the potential range of -0.2 to +0.5 V vs RHE before performing the experiments described in the paper.

## Supplementary Figures

Figure S1 – Pause-potential experiments from main-text Figure 1 plotted on time axis

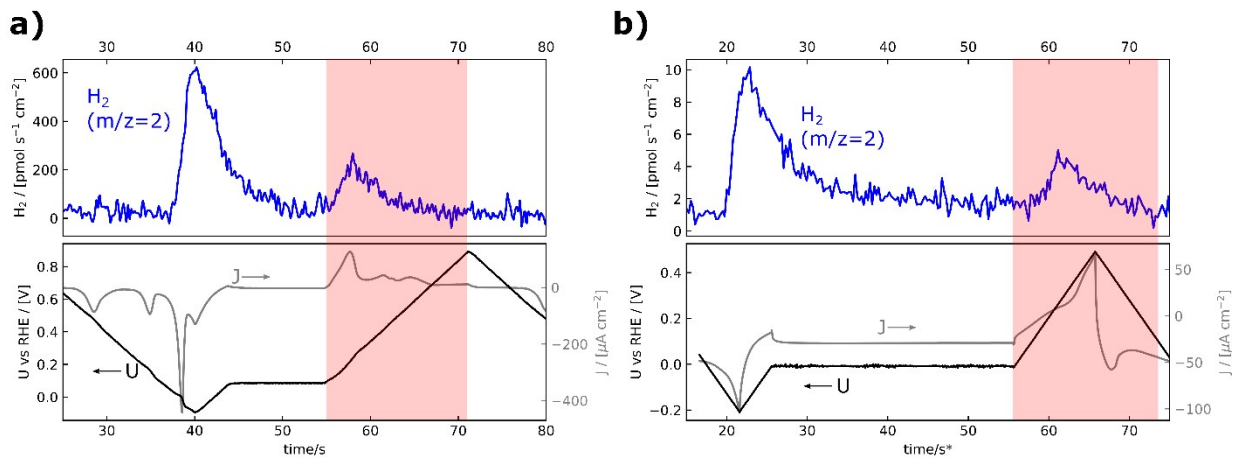
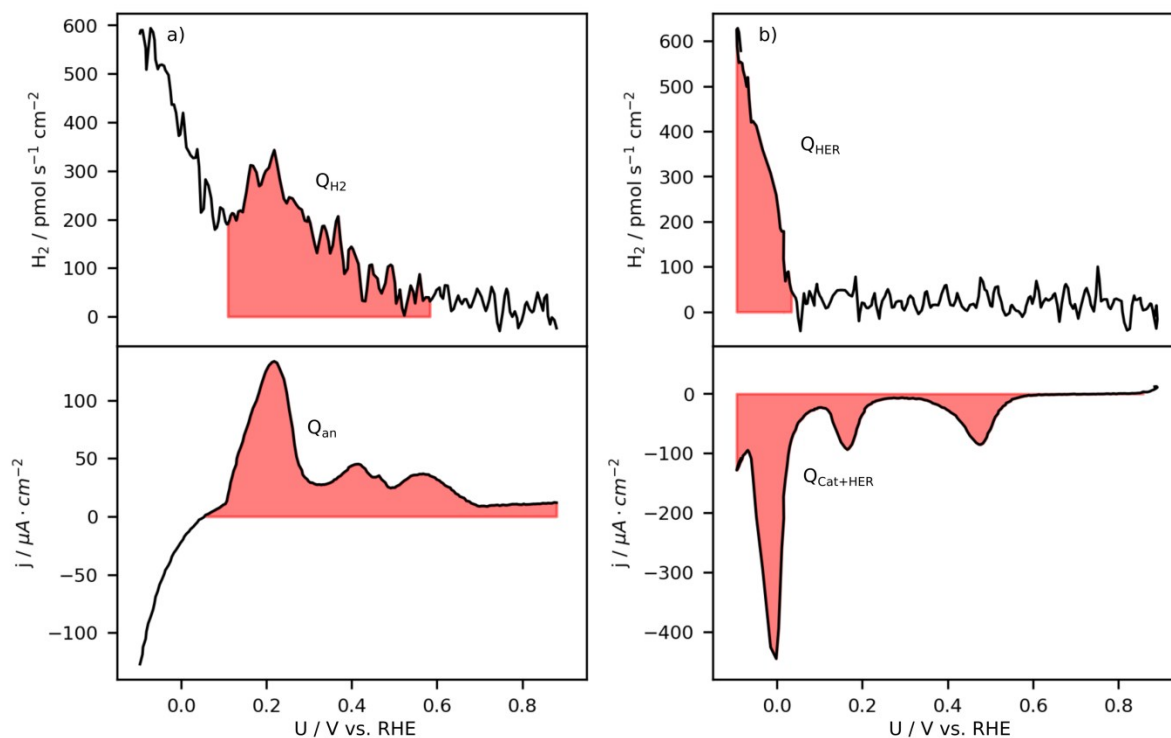


**Figure S1.**

Data from the red traces in Figure 1 of the main text, plotted vs potential, here plotted vs time. (a), Ru(0001) in 0.1 M HClO<sub>4</sub> and (b), Cu(pc) in 0.1 M KOH both at 50 mV/s. The m/z=2 signal, calibrated to a hydrogen flux, is plotted in the top panel. The electrochemistry data is plotted in the lower panel with potential on the RHE scale plotted against the left y-axis and current density on the left y-axis. The top and bottom panels share the same time axis. The portions of the experiments included as the red traces in main-text Figure 1 are indicated with a red highlight.

## Quantification of Ru(0001) charges.



Fi

### Figure S2

Representative CV (black trace from the manuscript in Figure 1a) is split in a positive- and negative-going scan in a) and b), respectively. Upper panels show the current traces of the CV and the lower panels the mass spectrometry signal. The areas for the charge evaluation are highlighted accordingly, both in the CV and the mass spectrometry signal.

The values for the charges presented in the manuscript for Ru(0001) electrodes are average values determined from several CVs recorded at different days. The procedure for the charge evaluation is described in the following based on Figure S2. The resulting values ( $\mu\text{C}\cdot\text{cm}^{-2}$ ) including the error ( $\mu\text{C}\cdot\text{cm}^{-2}$ ) and boundary conditions are summarized in Table S1. We also converted the charges into values of electrons transferred per surface atom ( $e^-/\text{atom}$ ), which are obtained by dividing the charges by  $256 \mu\text{C}\cdot\text{cm}^{-2}$ . This charge corresponds to the transfer of 1 electron per surface Ru atom, where the Ru atom density on the 0001 surface is  $1.6\cdot 10^{15} \text{ atoms}\cdot\text{cm}^{-2}$  and the Ru next neighbor distance is 0.27 nm. The anodic charge ( $Q_{\text{an}}$ ) passed in the CV has been determined from the positive-going scan of the BCV, for potentials where the current ( $j$ ) is positive. From the positive going scan of the  $m/z=2$  signal we determine the charge of  $\text{H}_2$  ( $Q_{\text{H}_2}$ ) formed at positive potentials, for potentials larger 0.1 V, corresponding to the rest potential  $U^{\text{R}}$  in the CV in the manuscript, and potentials smaller than 0.65 V. The amount of  $^*\text{H}$  on the surface is then twice the charge of  $Q_{\text{H}_2}$ . The charge related to the HER was determined from the negative going-scan of the  $m/z=2$  signal for potentials

smaller 0.1 V. The total cathodic charge ( $Q_{\text{cat+HER}}$ ) passed in the CV, which includes the contribution from HER, has been determined from the negative-going scan of the BCV for potentials where the current is smaller zero. Finally, the cathodic charge passed in the CV which is only related to surface reduction processes ( $Q_{\text{cat}}$ ) is determined by the difference between  $Q_{\text{cat+HER}}$  and  $Q_{\text{HER}}$ .

If all processes on the surface during the complete potential scan were reversible,  $Q_{\text{an}}$  should be equal to  $Q_{\text{cat}}$ , hence the charge difference ( $Q_{\text{diff}}$ ) should be equal to zero. We clearly observe a difference in the charge balance, where  $Q_{\text{an}}$  is smaller compared to  $Q_{\text{cat}}$  and hence a positive value for  $Q_{\text{diff}}$ . The difference in the charge between the positive- and negative-going scan, can only be rationalized when the  $\text{H}_2$  formed in the positive-going scan at potentials larger 0.1 V does not involve a charge transfer process. If  $Q_{\text{diff}}$  was only related to the formation of  $\text{H}_2$  it should be equal to  $Q_{\text{*H}}$ . The results show that  $Q_{\text{diff}}$  is slightly larger compared to  $Q_{\text{*H}}$ . The most plausible explanation for the difference is the contribution from oxygen reduction reaction (ORR) caused by trace amounts of  $\text{O}_2$  in the electrolyte solution, which can almost no be avoided with our experimental set-up. Also an underestimation of the  $\text{H}_2$  formed by HER due to tailing of the  $\text{H}_2$  signal, increases the value of  $Q_{\text{cat+HER}}$  and hence adds up to the difference. Thus we suggest that the actual \*H coverage lies in between  $Q_{\text{*H}}$  and  $Q_{\text{diff}}$ , i.e, 0.45 to 0.65 ML \*H. A value in that range is in perfect agreement with the value of 0.5 ML \*H determined from CO displacement measurements performed on Ru(0001) in a previous study.

**Table S1:** Charges determined from multiple CVs in different potential regions. See text for details

	Value / $\mu\text{C}\cdot\text{cm}^{-2}$	e-/atom	Boundary conditions / transformations
$Q_{\text{an}}$	$533 \pm 28$	$2.05 \pm 0.11$	$j > 0 \mu\text{A}\cdot\text{cm}^{-2}$
$Q_{\text{H}_2}$	$59 \pm 8$	$0.22 \pm 0.03$	$U > 0.1 \text{ V} \ \& \ U < 0.65 \text{ V}$
$Q_{\text{*H}}$	$118 \pm 16$	$0.45 \pm 0.06$	$Q_{\text{H}_2} * 2$
$Q_{\text{HER}}$	$367 \pm 56$	$1.41 \pm 0.21$	$U < 0.1 \text{ V}$
$Q_{\text{cat+HER}}$	$1065 \pm 51$	$4.09 \pm 0.19$	$j < 0 \mu\text{A}\cdot\text{cm}^{-2}$
$Q_{\text{cat}}$	$698 \pm 29$	$2.68 \pm 0.11$	$Q_{\text{cat+HER}} - Q_{\text{HER}}$
$Q_{\text{diff}}$	$165 \pm 16$	$0.63 \pm 0.06$	$Q_{\text{cat}} - Q_{\text{an}}$

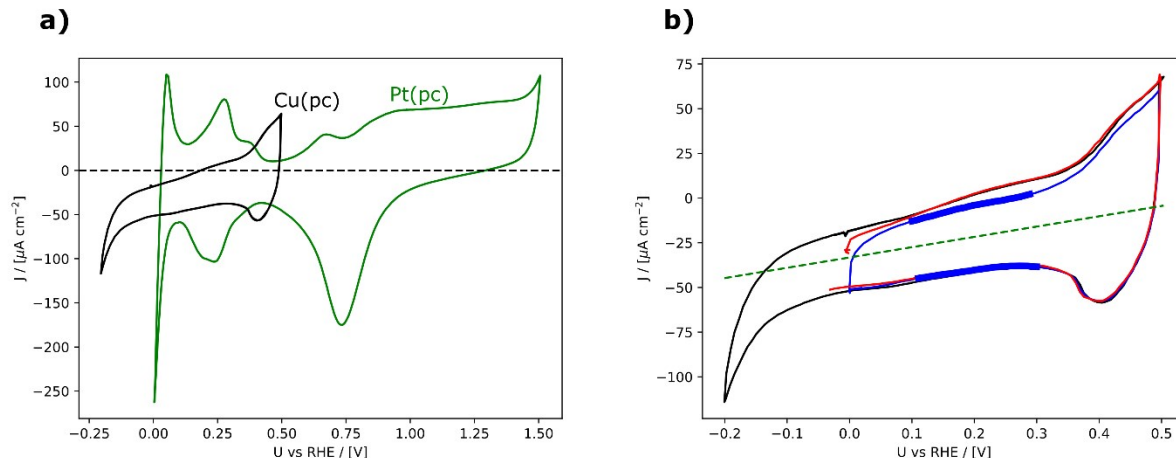


**Figure S3.**

(a) Polycrystalline Pt (green) and Cu (black) CV's taken in the chip EC-MS setup at 50 mV/s in the same 0.1 M KOH electrolyte under the same conditions with the same low  $m/z=32$  ( $\text{O}_2$ ) signal. The tilt is present in the Cu CV, whereas the Pt CV is more well-centered around zero and shows no tilt. This indicates that the tilt in the Cu(pc) CV is not due to  $\text{O}_2$  in the electrolyte. (b) For the analysis below, the tilt of the CV is treated as the result of an unwanted "shunt current" which is assumed to be linear with potential. The green dashed line is the line-of-best fit to the average of the cathodic and anodic scans in the portion of the CV without hydrogen adsorption (blue trace) between 0.1 V and 0.3 V (shown in bold traces). This green line is assumed to represent the shunt current.

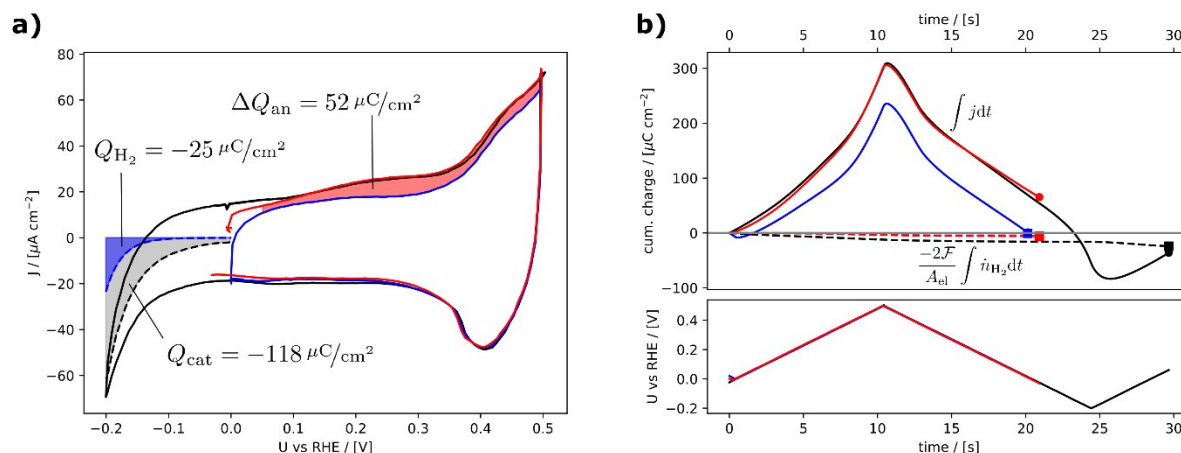


**Figure S4**

Charge balance for pc Cu. **(a)** Charge analysis of the three cyclic voltammograms from main-text Figure 1b. Here, the CV's have been corrected for tilt by subtracting the fit line shown in Figure S2b. The difference in current between the red trace (for which the sample had been brought to -0.2 V vs RHE and then held at 0 V vs RHE, see Figure S1b) and the blue trace, attributed to \*OH adsorption and/or Volmer \*H desorption, is highlighted in red. The average of the anodic and cathodic scans for the portion of the black trace below 0 V vs RHE is shown as a black dotted line, and the area under this line is highlighted. The total charge associated with the measured H<sub>2</sub> during the full CV is indicated as well in blue. The blue dotted trace indicates the H<sub>2</sub> production assuming that H<sub>2</sub> production (not necessarily desorption) has a Tafel slope of 60 mV/decade, with the pre-factor adjusted so that the area corresponds to the measured H<sub>2</sub> over the course of one cycle. The charges passed in all three highlighted areas are indicated. Note that the gray and blue highlighted areas imply charge passed on both the anodic and cathodic scans, and so are multiplied by 2 and divided by the scan rate to get  $Q_{\text{cat}}$  and  $Q_{\text{H}_2}$ , respectively. **(b)** The integrated charges (top panel, solid traces) and the integrated charge associated with the measured hydrogen signals (top panel, dotted traces) for each of the three experiments from main-text Figure 1b.

The quantitative analysis is split up below into analysis of the mass spectrometer signal (MS) and the electrochemical signal (EC)

MS: The anodic hydrogen desorption, taken to be the integrated H<sub>2</sub> signal in the red trace in main-text Figure 1 corresponds to approximately 26 pmol/cm<sup>2</sup>. Assuming the average surface site density of the most stable facets (111, 100, and 110), 2.4 nmol/cm<sup>2</sup>, this corresponds to approximately 1.0 % of a monolayer. The integrated H<sub>2</sub> signal in the black trace of main-text Figure 1 is 125 pmol/cm<sup>2</sup>, of which approximately 100 pmol/cm<sup>2</sup> conventional HER and the remainder is anodic hydrogen desorption.

EC: The net charge passed in the black trace cathodic of -0.1 V vs RHE, excluding that associated with the tilt of the CV (see the Supplementary Information,

Figure SX, for details), is approximately  $-100 \mu\text{C}/\text{cm}^2$ , corresponding to about 0.4 charges per surface atom. However, the total integrated  $\text{H}_2$  signal (cathodic HER and anodic  $\text{H}_2$  desorption) in the black trace is only about  $135 \text{ pmol}/\text{cm}^2$ , corresponding to 5% of a monolayer of  $\text{H}_2$  or 0.1 charges per surface atom. Most of the difference is made up by the charge associated with the broad anodic peak starting at  $+0.1 \text{ V}$  vs RHE, which (using the blue trace as a background) is  $50 \mu\text{C}$ , or about 0.2 charges per surface atom. This implies that a significant  $^*\text{H}$  coverage is formed at the onset of HER on Cu(poly), most of which is oxidized in the subsequent anodic scan and some of which is desorbed as  $\text{H}_2$ . Further studies are needed to improve this preliminary quantitative analysis.

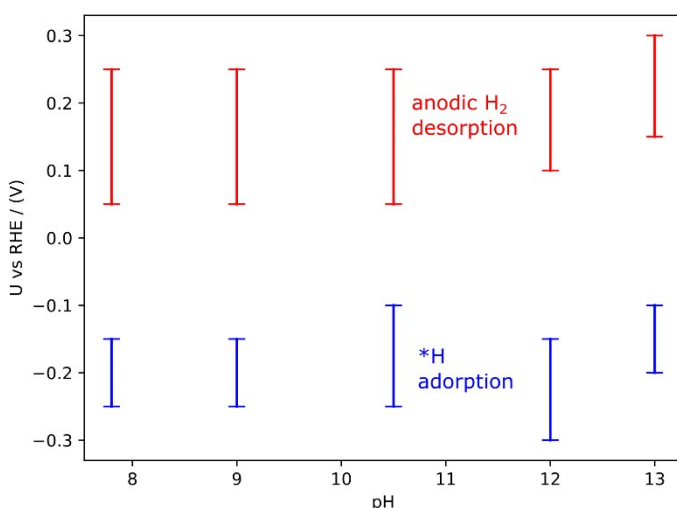


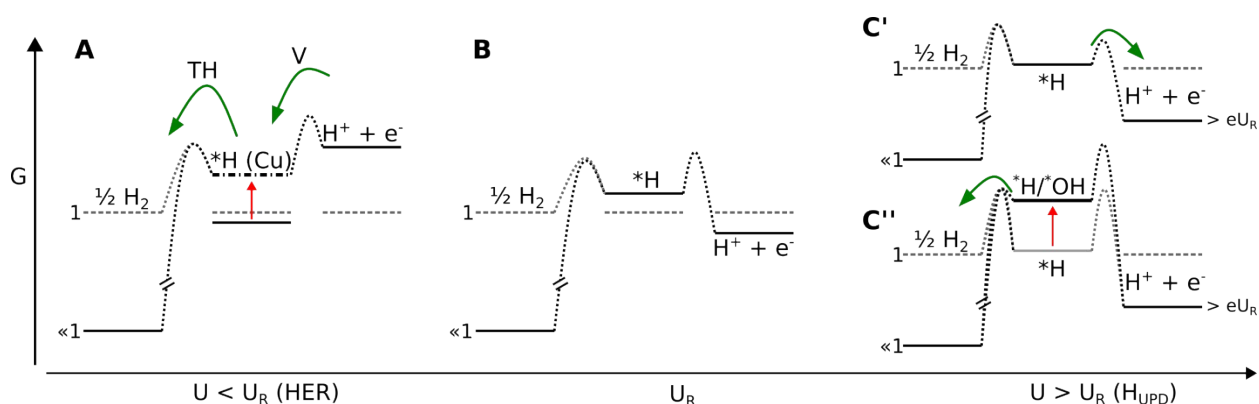
**Figure S5**

Hydrogen adsorption and desorption vs pH.

The ranges were found by cyclic voltammetry changing the anodic or cathodic potential limits. The anodic H<sub>2</sub> desorption range (red) is defined as the potential range in which the size of the anodic H<sub>2</sub> desorption mass spectrometer signal depended on the anodic potential limit, while the cathodic potential limit was held constant at -0.3 V vs RHE. With an anodic potential limit below the lower end of this range, no anodic hydrogen evolution was observed, and with an anodic potential limit above the high end of this range, increasing the anodic potential limit did not effect the amount of anodic H<sub>2</sub> desorption signal. Similarly, the \*H adsorption potential range (blue) is defined as the potential range in which the size of the anodic H<sub>2</sub> desorption mass spectrometer signal depended on the cathodic potential limit, while the anodic potential limit was held constant at +0.5 V vs RHE. If the cathodic potential limit was above the high end of this range, no anodic hydrogen desorption was observed. If the cathodic potential limit was below the low end of this range, the anodic hydrogen desorption signal no longer increased as a result of decreasing cathodic potential. Note that conventional HER, i.e. *cathodic* hydrogen desorption, started at all pH's at a lower potential than the high end of the \*H adsorption range, and increased with decreasing cathodic potential limit beyond the low end of the \*H adsorption range. In this way, anodic hydrogen adsorption is used as a probe of \*H adsorption, independent of cathodic HER.

The electrolyte for pH=13 was 0.1 M KOH. The electrolyte pH 7.8 was CO<sub>2</sub>-saturated 1 M KHCO<sub>3</sub>. The electrolytes for the intermediate pH values were formed by mixing these two electrolytes in the needed ratio, calculated by the carbonate-bicarbonate equilibrium as described in Reference <sup>6</sup>.

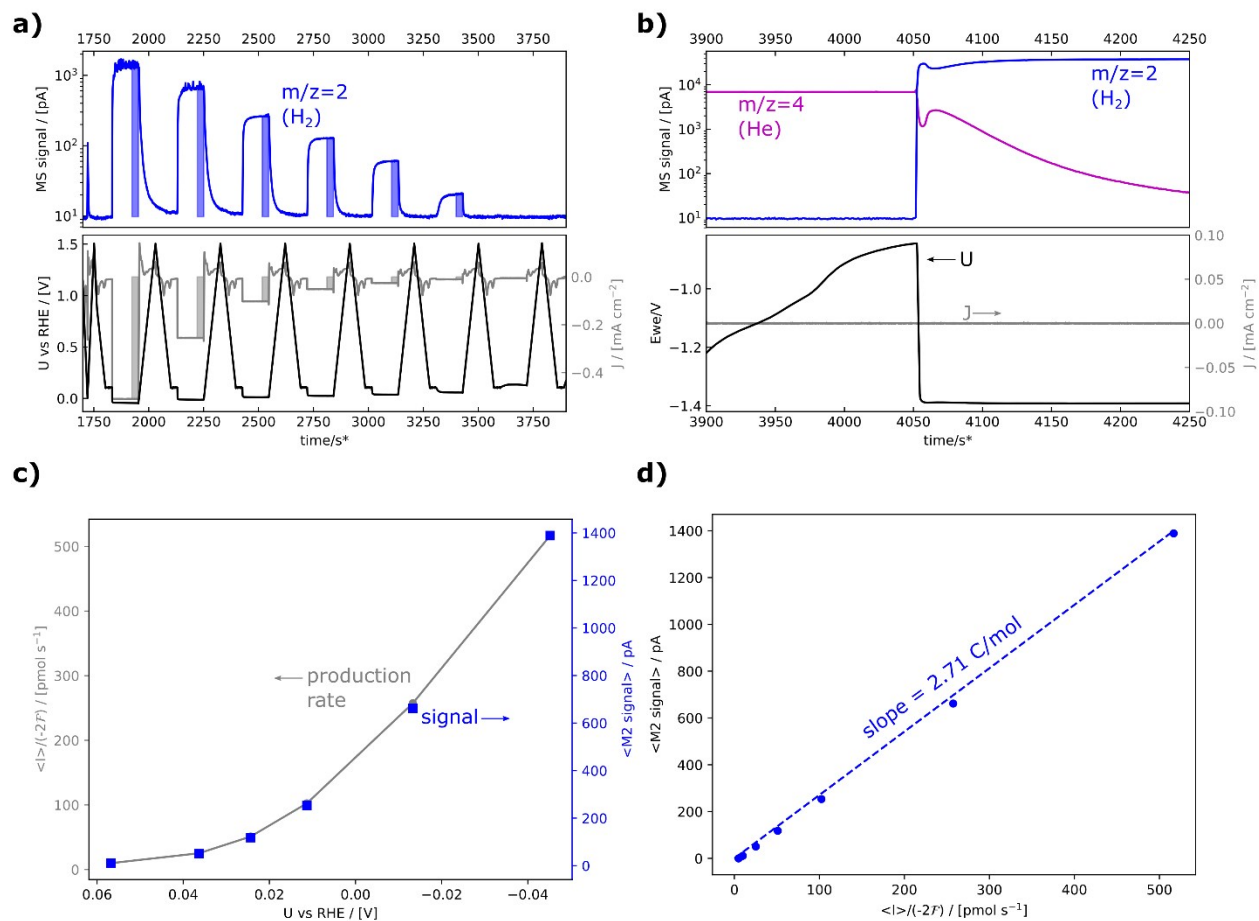
In conclusion, the cathodic adsorption of \*H and its anodic desorption as H<sub>2</sub> are pH-independent on the RHE scale.



**Figure S6**

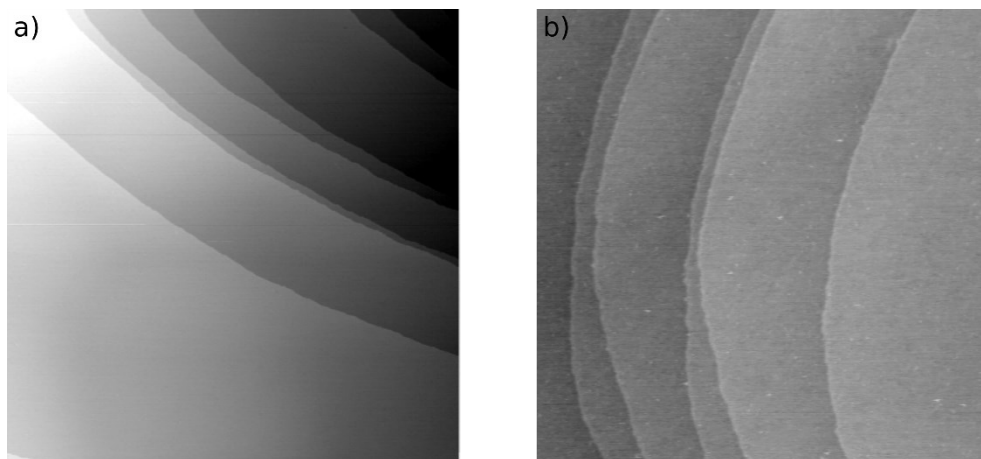
Sketches of the free energy landscapes for the Volmer (**V**) and Tafel/Heyrovsky (**TH**) steps including kinetic barriers for Cu(pc) at three potentials. Green arrows indicate the dominant reaction path. The  $\frac{1}{2} \text{H}_2$  free energy levels are denoted by 1 and  $\ll 1$ , for standard equilibrium conditions and non-standard conditions in an open system with a lower  $\text{H}_2$  partial pressure, respectively. The levels for  $U^0_{\text{H}_2/2\text{H}^+}$  under standard conditions are marked as dashed lines. The red arrow in panel A indicates the change in the free energy level of  $^*\text{H}$  with increasing  $^*\text{H}$  coverage (dash dotted line). Panel B corresponds to  $U_{\text{R}}$  (rest potential in Figure 1, 0.0 V vs RHE for Cu(pc)). Panel C' and C'' describe the situation at potentials  $> U_{\text{R}}$ . The red arrow indicates the change in the free energy level of  $^*\text{H}$  when taking  $^*\text{OH}$  adsorption into account.

Figure S6 sketches the energy landscape, corresponding to main-text Figure 3, as we understand it for Cu(pc). The main difference, compared to Ru(0001), is that the energy for  $^*\text{H}$  is shifted to much higher values. At least some  $^*\text{H}$  remains trapped on the surface as the potential is scanned anodic past  $U_{\text{R}}$ , however, due to the large barriers for the elementary steps.



**Figure S7**

Calibration with Pt. **(a)** H<sub>2</sub> calibration with constant-current steps separated by CV's and **(b)** RHE potential calibration by introducing H<sub>2</sub> through the chip. The procedures are described in Reference <sup>7</sup>. **(c)** and **(d)** are analysis of the H<sub>2</sub> calibration. The slope in **(d)**, 2.71 C/mol, is the sensitivity factor of the mass spectrometer for H<sub>2</sub> at  $m/z=2$ .



**Figure S8**

STM images (400 nm x 400 nm) of Ru(0001) measured under UHV conditions a) before and b) after the electrochemical characterization. Tunneling parameters are a)  $U_T = 1.0 - 1.5$  V,  $I_T = 0.5 - 10$  nA and b)  $U_T = 50 - 100$  mV,  $I_T = 0.5 - 10$  nA.

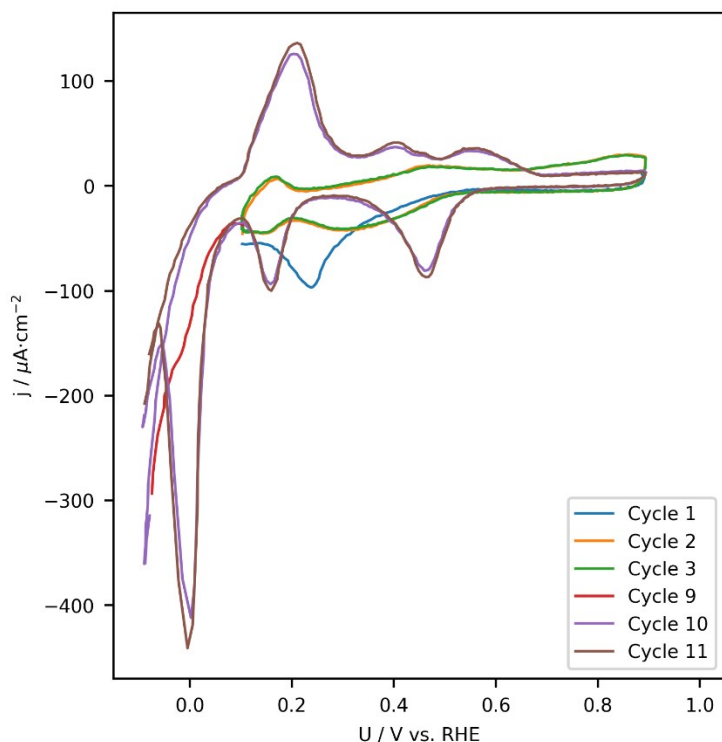


**Figure S9**

First potential cycles recorded on a Ru(0001) in 0.1 M HClO<sub>4</sub> at 50 mV/s.

The first cycles were recorded in a potential range between 0.1 V and 0.9 V. The very first cycle shows a reduction peak at ca. 0.25 V, while the following cycles (only second and third shown) show a stable CV. The CV does not show pronounced features as expected for a Ru(0001) electrode. Instead the CV has strong resemblance to a CV recorded on RuO<sub>2</sub>(110) thin films supported on Ru(0001) reported elsewhere<sup>8</sup>. Upon decreasing the lower potential limit to -0.1 V (Cycle 9, red trace), a shoulder appears in the HER region and in the subsequent cycles (Cycles 11 and 12) the CV shows the distinct features for bare Ru(0001) electrodes recorded in 0.1 M HClO<sub>4</sub>, as shown in previous studies<sup>3,9</sup>. We assume that the initial electrode is covered by an oxide layer, resulting from oxidation of the electrode (i) during the transfer from trace amounts of O<sub>2</sub> present in the gas phase, before immersing the electrode in the electrolyte and (ii) by keeping the electrode for approximately 30-60 s at open circuit potential in the electrolyte before starting the actual measurement. Note that in the current set up we are not able to immerse the electrodes under potential control. According to the STM images presented in Figure S8, we suggest that the reduction of this oxide layer does not change the electrode surface significantly.

## References

- (1) Kopatzki, K. E. PhD Thesis, Sauerstoffadsorption, Oxidbildung und Homoepitaxie auf Ni(100) Oberflächen - eine Untersuchung mit dem Rastertunnelmikroskop **1994** University München.
- (2) Engstfeld, A. K.; Klein, J.; Brimaud, S.; Behm, R. J. Electrochemical Stability and Restructuring and Its Impact on the Electro-Oxidation of CO: Pt Modified Ru(0001) Electrodes. *Surf. Sci.* **2015**, *631*, 248–257.
- (3) El-Aziz, A. .; Kibler, L. . New Information about the Electrochemical Behaviour of Ru(0001) in Perchloric Acid Solutions. *Electrochem. commun.* **2002**, *4*, 866–870.
- (4) Schnaidt, J.; Beckord, S.; Engstfeld, A. K.; Klein, J.; Brimaud, S.; Behm, R. J. A Combined UHV-STM-Flow Cell Set-up for Electrochemical/Electrocatalytic Studies of Structurally Well-Defined UHV Prepared Model Electrodes. *Phys. Chem. Chem. Phys.* **2017**, *19*, 4166–4178.
- (5) Trimarco, D. B.; Scott, S. B.; Thilsted, A. H.; Pan, J. Y.; Pedersen, T.; Hansen, O.; Chorkendorff, I.; Vesborg, P. C. K. Enabling Real-Time Detection of Electrochemical Desorption Phenomena with Sub-Monolayer Sensitivity. *Electrochim. Acta* **2018**.
- (6) Scott, S. B. Investigating the Electrochemical Reduction of Carbon Dioxide Using In Situ Mass Spectrometry, Technical University of Denmark, 2016.
- (7) Scott, S. B. Isotope-Labeling Studies in Electrocatalysis for Renewable Energy Conversion, and the Net Carbon Impact of This PhD Project, Technical University of Denmark, 2019.
- (8) Weber, T.; Abb, M. J. S.; Khalid, O.; Pfrommer, J.; Carla, F.; Znaiguia, R.; Vonk, V.; Stierle, A.; Over, H. In Situ Studies of the Electrochemical Reduction of a Supported Ultrathin Single-Crystalline RuO<sub>2</sub> (110) Layer in an Acidic Environment. *J. Phys. Chem. C* **2019**, *123*, 3979–3987.
- (9) Alves, O. B.; Hoster, H. E.; Behm, R. J. Electrochemistry at Ru(0001) in a Flowing CO-Saturated Electrolyte—Reactive and Inert Adlayer Phases. *Phys. Chem. Chem. Phys.* **2011**, *13*, 6010.